Available online at www.sciencedirect.com
ScienceDirect
Journal of Power Sources 173 (2007) 774–780
JOURNAL OF POWER SOURCES
www.elsevier.com/locate/jpowsour

# Thin film $TiO_2$ photoanodes for water photolysis prepared by dc magnetron sputtering

A. Brudnik [b], A. Gorzkowska-Sobaś [a], E. Pamuła [a], M. Radecka [a,*], K. Zakrzewska [b]

[a] *Faculty of Material Science and Ceramics, AGH-University of Science and Technology, Al. Mickiewicza 30, 30-059 Kraków, Poland*
[b] *Faculty of Electrotechnics, Automatics, Computer Science and Electronics, AGH-University of Science and Technology, Al. Mickiewicza 30, 30-059 Kraków, Poland*

Available online 26 May 2007

**Abstract**

The $TiO_2$ thin film photoanodes for hydrogen generation by water photolysis have been prepared by dc reactive magnetron sputtering. Optical monitoring of the plasma emission with the feedback signal $I/I_0$ controlling the reactive gas admission and reflecting the target oxidation state has been used. X-ray diffraction GID and AFM studies have revealed the systematic evolution of the microstructure with $I/I_0$, from that of well-crystallized mixture of anatase and rutile at the lowest $I/I_0$ (oxidized target) to that of amorphous state with finely dispersed rutile grains at the highest $I/I_0$ (metallic target). It has been demonstrated that the microstructure of $TiO_2$ affects to a large extent the optical and photoelectrochemical properties of the photoanodes. Optical band gap $E_{opt}$ and the photocurrent response have been found to increase systematically with a decreasing feedback signal $I/I_0$. The best efficiency, i.e. the highest IPCE (incident photon-to-current conversion efficiency) has been obtained for the $TiO_2$ photoanodes sputtered at $I/I_0 = 0.09$ from the oxidized target.


*Keywords:* Photoelectrochemical cell (PEC); Water photolysis; Titanium dioxide; Reactive dc magnetron sputtering

## 1. Introduction

Negative environmental aspects of utilizing fossil fuels give rise to a widespread demand to replace the traditional energy sources with renewable ones, such as solar, wind and hydro-energy. Among numerous devices for solar energy conversion, a photoelectrochemical cell (PEC) allows for the photocatalytic decomposition of water, during which pure, gaseous hydrogen and oxygen are released. Thus, hydrogen produced in PEC by means of water photolysis serves as an excellent example of the future fuel [1,2]. Typically, PEC consists of an n-type semiconducting photoanode and a metallic cathode, immersed in a water solution of an electrolyte [3]. Light absorbed by the photoanode results in the intrinsic ionization of the semiconductor over its energy band gap $E_g$, leading to creation of electrons $e'$ in the conduction band and electron holes $h^\bullet$ in the valence band, according to

$$h\nu \rightarrow h^\bullet + e' \quad (1)$$

The photogenerated charge carriers are then separated by the electric field, existing near the surface of the semiconducting photoanode. The holes oxidize water molecules at the anode:

$$2h^\bullet + H_2O \rightarrow \tfrac{1}{2}O_2 + 2H^+ \quad (2)$$

The electrons are transported through the external circuit to the cathode, where the reduction of $H^+$ proceeds:

$$2e' + 2H^+ \rightarrow H_2 \quad (3)$$

PEC for water photoelectrolysis is depicted schematically in the diagram (Fig. 1).

Titanium dioxide is considered to be the most promising photoanode material [4] thanks to its:

- chemical stability,
- high resistance to corrosion and photocorrosion,
- non-toxicity,
- favorable positions of the valence and conduction band edges with respect to the reduction and oxidation potentials of water.

However, due to a relatively wide band gap $E_g$, the optical absorption spectrum of $TiO_2$ does not match a solar spectrum and

* Corresponding author. Tel.: +48 12617 25 26; fax: +48 12617 24 93.
*E-mail address:* radecka@agh.edu.pl (M. Radecka).

0378-7753/$ – see front matter © 2007 Elsevier B.V. All rights reserved.
doi:10.1016/j.jpowsour.2007.05.084

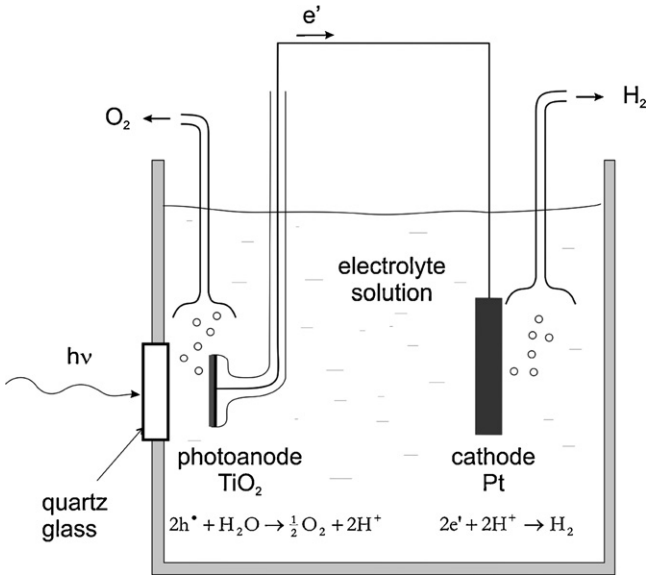


Fig. 1. Photoelectrochemical cell PEC for water photoelectrolysis.

the PEC with $TiO_2$ photoanodes exhibits rather poor efficiency of the solar energy conversion [4,5]. It should be emphasized that the efficiency of water photolysis depends on the intrinsic properties of the materials applied as the photoelectrodes, especially on their microstructure which affects the recombination rate of photogenerated electrons and holes [6]. Moreover, it has been shown that the photoelectrochemical current–voltage (*I–V*) characteristics and photocurrent spectra can be improved by a proper modification of the microstructure of the photoanode material [6,7]. Therefore, the microstructure of the photoanode affects to a large extent the PEC performance.

In order to increase a surface-to-volume ratio, $TiO_2$ photoanodes are usually prepared as thin films. The majority of the films properties are susceptible to the preparation method and technological parameters of the deposition process. $TiO_2$ thin film photoanodes for PEC are frequently obtained by means of sol–gel technique [7–10], while the reactive sputtering of metallic targets is widely used for other photocatalytic applications, such as self-cleaning surfaces covered by the photocatalytically active $TiO_2$ [11,12]. Also, because the sputtering techniques are highly efficient and provide a large throughput, they are often used for industrial applications [13]. In our work we have chosen magnetron sputtering with the pulsed dc power supply, as a high rate sputtering technique, to deposit $TiO_2$ onto Ti foil in order to produce photoanodes suitable for PEC. The photoanodic behavior of the thin films obtained by this technique has not been yet systematically studied in the literature.

High rate reactive sputtering from metallic targets in $Ar + O_2$ atmosphere suffers from an uncontrollable switching between two stable modes of operation: (1) when target is completely oxidized, so-called "oxide" mode and (2) when target is clean of the oxides, so-called "metallic" mode. The access to the transition region between these stable modes is required since it provides oxide layers with different metal to oxygen ratio at sufficiently high rates [14–16]. However, the instability between the sputtering rate and oxygen partial pressure prevents the operation within the transition region under standard conditions. In order to overcome this instability and perform the sputtering at an intermediate point within the transition region, an active process feedback is necessary [14–17]. In this work, the optical monitoring of the plasma emission with the feedback signal controlling the reactive gas admission has been used. In our earlier papers [16,18,19] we have shown that high rate sputtering sources, such as magnetrons, offer a unique possibility for tailoring the microstructure of $TiO_2$ thin films in respect to a phase composition, anatase to rutile ratio and nonstoichiometry in a reproducible and controllable way. The oxidation state of the sputtered target is expected to affect the departure from stoichiometry in the growing films of $TiO_2$. Our earlier Rutherford backscattering RBS and nuclear reactions analysis, NRA studies have demonstrated systematic changes in the departure from stoichiometry for films deposited from metallic surfaces [18,19]. In this paper the emphasis is put on a correlation between the photocurrent response of the $TiO_2$ photoanodes fabricated by dc reactive magnetron sputtering and the controlled sputtering conditions. The aim of this paper is to elucidate the main factors responsible for the changes observed in the efficiency of the photoelectrolysis process as well as to establish the technological conditions responsible for the best performance of PEC with $TiO_2$ photoanodes prepared by plasma-emission-controlled dc magnetron sputtering.

## 2. Experimental

The films were prepared in a planar, balanced magnetron sputtering system. Metallic Ti target of purity 99.95% was sputtered in an $Ar + O_2$ reactive gas atmosphere in a closed-loop system with the optical control. The deposition arrangement was vertical and the magnetron discharge was driven by a dc-pulse supply.

The applied optical control system is based on the plasma emission and uses the relative ratio of the intensity $I/I_0$ of Ti emission line as the only parameter, so-called feedback parameter, that controls the sputtering rate through its influence on the target oxidation state. The intensity $I$ of Ti emission line at $\lambda = 500$ nm at a given $Ar + O_2$ is monitored continuously and serves as a feedback signal for the gas admission. The line intensity $I_0$ corresponds to pure metallic deposition mode at 100% Ar. The interference filter with a bandpass width of $\pm 5$ nm is used to extract the desired line from the magnetron cathode plasma ring. The emitted light is detected from the region of about 5 mm below the target, while the target-to-substrate distance is 50 mm.

$TiO_2$ thin films were obtained at different feedback parameters $I/I_0$. The working pressure was $1.5 \times 10^{-2}$ hPa and the power density was 15 W cm$^{-2}$. The substrate temperature was kept constant at 520 K. For the optical absorption measurements a quartz glass was used as a transparent substrate and the $TiO_2$ photoanodes were deposited onto the metallic titanium foil (0.127 mm thick, 99.98% pure, Sigma–Aldrich). The thickness of the samples was determined mechanically by a Talystep profilometer. Sputtering conditions are given in Table 1.

Standard techniques were applied to characterize the samples. Structural information was obtained from X-ray diffraction

Table 1
Technological conditions (sputtering parameters) for dc magnetron sputtering with plasma emission control system

| Feedback parameter, $I/I_0$ | Time of deposition (s) | Film thickness, $d$ (nm) | Growth rate (nm s$^{-1}$) |
|---|---|---|---|
| 0.40 | 240 | 280 | 1.2 |
| 0.30 | 350 | 300 | 0.9 |
| 0.25 | 440 | 300 | 0.7 |
| 0.20 | 670 | 390 | 0.6 |
| 0.15 | 726 | 320 | 0.4 |
| 0.10 | 1110 | 270 | 0.2 |
| 0.09 | 1200 | 320 | 0.3 |

measurements on an X'Pert MPD Phillips diffractometer at grazing incidence (GID). The surface topography was analyzed by means of the atomic force microscope Explorer (ThermoMicroscopes, Vecco, USA). The images were recorded in contact mode, as 5 μm × 5 μm scan areas (300 × 300 data points) and with a scan rate of 3 lines s$^{-1}$. All images were flatten using a software SPMlab602 and presented as 2D and 3D projections. Cross-sectional and roughness analyses were also performed.

Optical measurements were carried out on a Perkin-Elmer Lambda 19 double beam spectrophotometer over 200–2200 nm wavelength range. The transmittance T(λ) and the reflectance R(λ) spectra served for the optical band gap $E_{opt}$ calculations. The $E_{opt}$ values were obtained from the so-called Tauc's plot, i.e. the plot of $(\alpha h\nu)^{1/\gamma}$ versus photon energy $h\nu$, where $\gamma = 2$ is assumed for the amorphous non-metallic materials [20].

The as-sputtered $TiO_2$ thin film photoanodes were then placed in the PEC, together with the metallic cathode, i.e. a platinum foil covered with platinum black, and a saturated calomel electrode (SCE) working as a reference electrode. The electrodes were immersed in a phosphoric buffer solution of pH 7.7. A 450 W Xe Osram lamp with a Jobin Yvon monochromator TRIAX 180 was used for the photoanode illumination.

The photocurrent response to the white light and the photocurrent spectra $I_{ph}(\lambda)$ were measured for the unbiased electrodes using a Keithley 6517A electrometer. The current–voltage ($I_{ph}$–$V$) characteristics were recorded with an ANKO potentiostat for the photoanodes illuminated with the white light. The flat band potential $V_{fb}$ was obtained from the $I_{ph}$–$V$ curves and assumed to be equal to the potential value at the onset of the anodic photocurrent [21]. The experimental points for the $I_{ph}(\lambda)$ characteristics were taken when the photocurrent at a given wavelength λ had reached a constant level. The spectral photocurrent responses were used in calculations of the incident photon-to-current conversion efficiency (IPCE), according to the formula given by Gerischer [22]:

$$\mathrm{IPCE}\,(\%) = \frac{1240 I_{ph}}{\lambda W_\lambda} \tag{4}$$

where $I_{ph}$ is the photocurrent density at a particular wavelength and $W_\lambda$ is the intensity of light.

## 3. Results and discussion

The analysis of GID patterns reveals that the films are composed of two $TiO_2$ polymorphic forms: anatase and rutile, accompanied by an amorphous phase. As can be seen in Fig. 2, the sputtering conditions affect the GID patterns and the relative intensities of A(1 0 1) anatase and R(1 1 0) rutile diffraction lines vary with the feedback parameter $I/I_0$ that reflects the oxidation state of the target. For the lowest $I/I_0 = 0.09$, when the target is oxidized, the films show the highest degree of crystallization. Under these conditions both anatase and rutile phases occur, with anatase as a dominating phase. With the increasing $I/I_0$ the surface of the target becomes less oxidized and a systematic evolution of the microstructure is observed, i.e. the rutile content increases, while the anatase phase gradually disappears. For the films sputtered at $I/I_0 = 0.32$, a high sputtering rate and a metallic-like surface of the target promote rutile growth and the anatase phase is not detected. A further increase in the $I/I_0$ leads to a broadening of R(1 1 0) diffraction line for $I/I_0 = 0.35$, suggesting that the film becomes amorphous with finely dispersed rutile grains. The amorphous phase predominates at the highest $I/I_0$ ($I/I_0 = 0.40$), making the diffraction pattern obtained for this sample practically featureless.

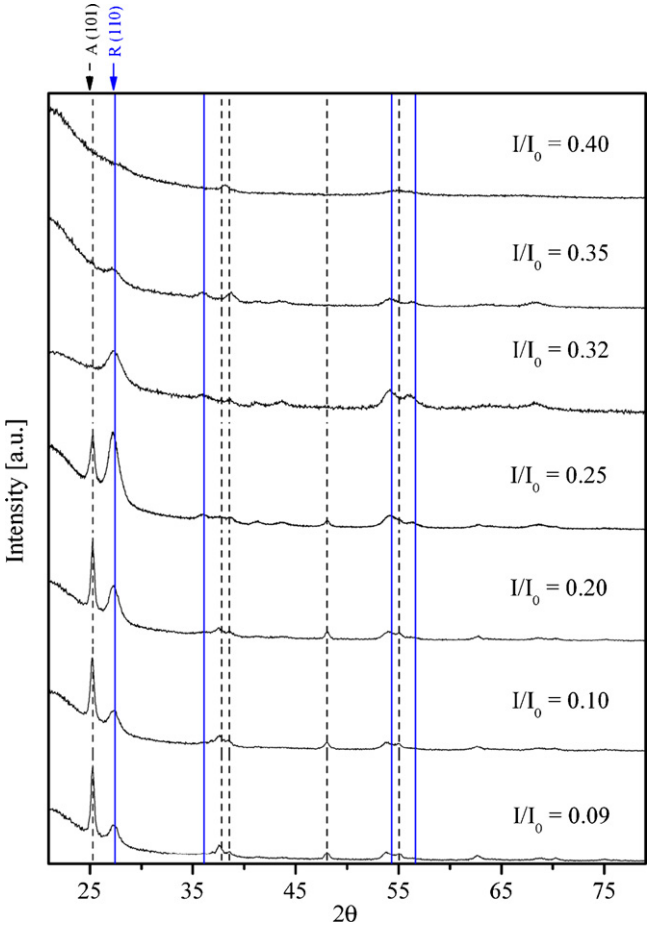


Fig. 2. X-ray diffraction patterns of $TiO_2$ thin film photoanodes obtained by reactive sputtering from Ti target at different feedback parameters $I/I_0$.

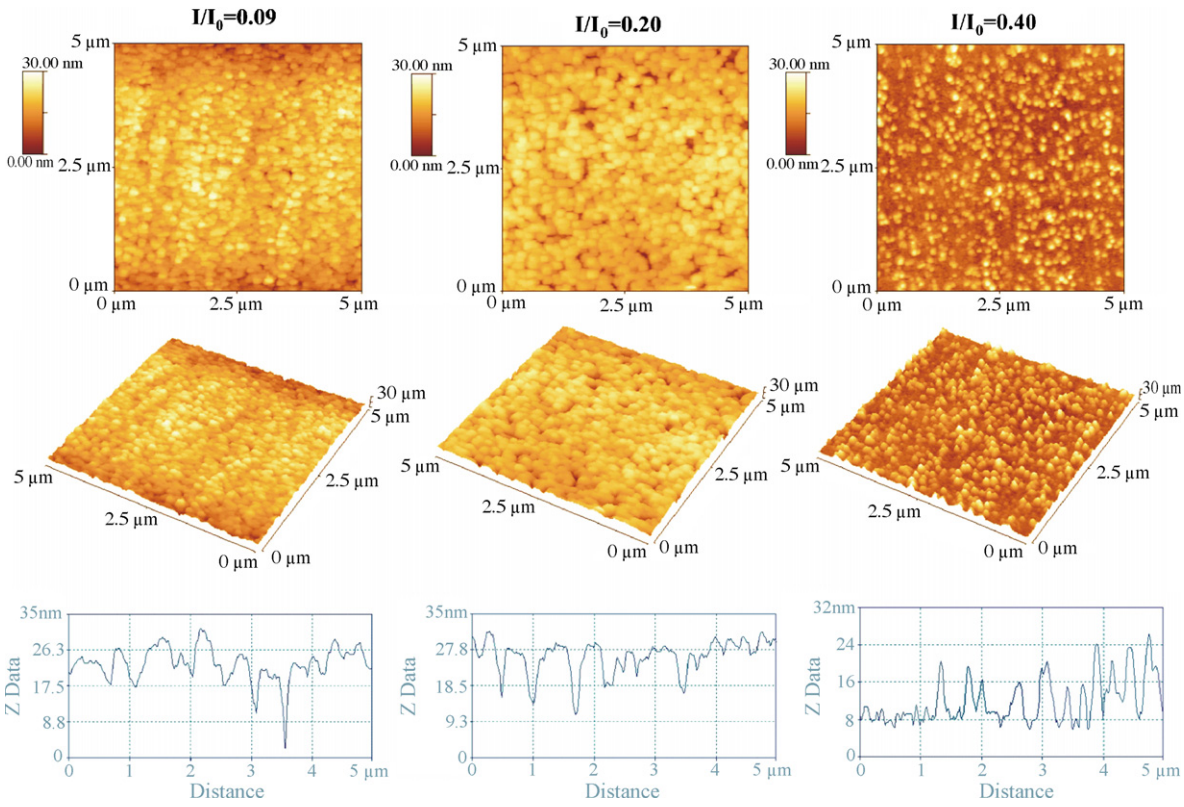


Fig. 3. AFM topographic images (2D and 3D projections) of $TiO_2$ thin film photoanodes obtained by sputtering from Ti target at different feedback parameters $I/I_0$. Cross sections taken along horizontal lines in the centres of the images are also shown.

The AFM images shown in Fig. 3 are in agreement with the results of the X-ray analysis. The film obtained at $I/I_0 = 0.40$ consists of randomly dispersed, isolated surface features of nanometric dimensions. The height of those features is between 10 and 15 nm as follows from cross-section analysis. A decrease in $I/I_0$ results in an increase in surface density of these features, while the films become more compact. This is a direct consequence of the enhanced crystallization, as seen in Fig. 2. The average surface roughness $R_{rms}$ is close to 4.3 nm and remains unaffected by the changes in $I/I_0$.

The optical properties have been found equally sensitive to the changes in the oxidation state of the sputtered target. Fig. 4 presents transmittance T(λ) and reflectance R(λ) spectra for $TiO_2$ thin films deposited at different $I/I_0$. The films sputtered at $I/I_0 = 0.09$, when the target is oxidized, are optically uniform and are characterized by the high transmittance over the visible range of the light spectrum. The optical absorption edge of these films is relatively sharp and corresponds to the absorption edge of stoichiometric $TiO_2$. When $I/I_0$ increases above 0.25 and the target undergoes a progressive evolution to the metallic state, the average transmittance of the films decreases over the visible range. The additional absorption band is formed at about 1–2 eV. The results of the RBS and NRA analysis [19] revealed that a departure from stoichiometry increased with the increasing $I/I_0$ for $I/I_0 > 0.25$. On the contrary, no systematic changes in the departure from stoichiometry could be detected for the films deposited at $I/I_0 < 0.25$ [19]. Therefore, the absorption band occurring over the visible range can be accounted for by additional electronic states formed within the forbidden band gap of $TiO_2$ that result from the oxygen nonstoichiometry.

The values of the optical energy band gap $E_{opt}$, obtained from the Tauc's plots are listed in Table 2. The $E_{opt}$ increases with the decreasing $I/I_0$. It should be pointed out, that $E_{opt}$ for $TiO_2$ rutile is of about 3.0 and 3.2 eV for the anatase. Thus, the rise in the optical band gap with the decreasing $I/I_0$ can be related to the growing anatase content in the films.

The changes in nonstoichiometry and the microstructure of the films are followed closely by the photoelectrochemical properties. Dynamic photocurrent response of the photoanode is due to the photogeneration of charge carriers and relaxation mechanism in $TiO_{2-x}$ films.

Table 2
Optical energy band gap values $E_{opt}$ for $TiO_2$ films sputtered at different feedback parameters $I/I_0$

| Feedback parameter, $I/I_0$ | Optical band gap, $E_{opt}$ (eV) |
|---|---|
| 0.35 | 3.03 ± 0.01 |
| 0.32 | 3.04 ± 0.01 |
| 0.28 | 3.12 ± 0.01 |
| 0.25 | 3.21 ± 0.01 |
| 0.20 | 3.20 ± 0.02 |
| 0.15 | 3.20 ± 0.01 |
| 0.10 | 3.26 ± 0.01 |
| 0.09 | 3.28 ± 0.01 |

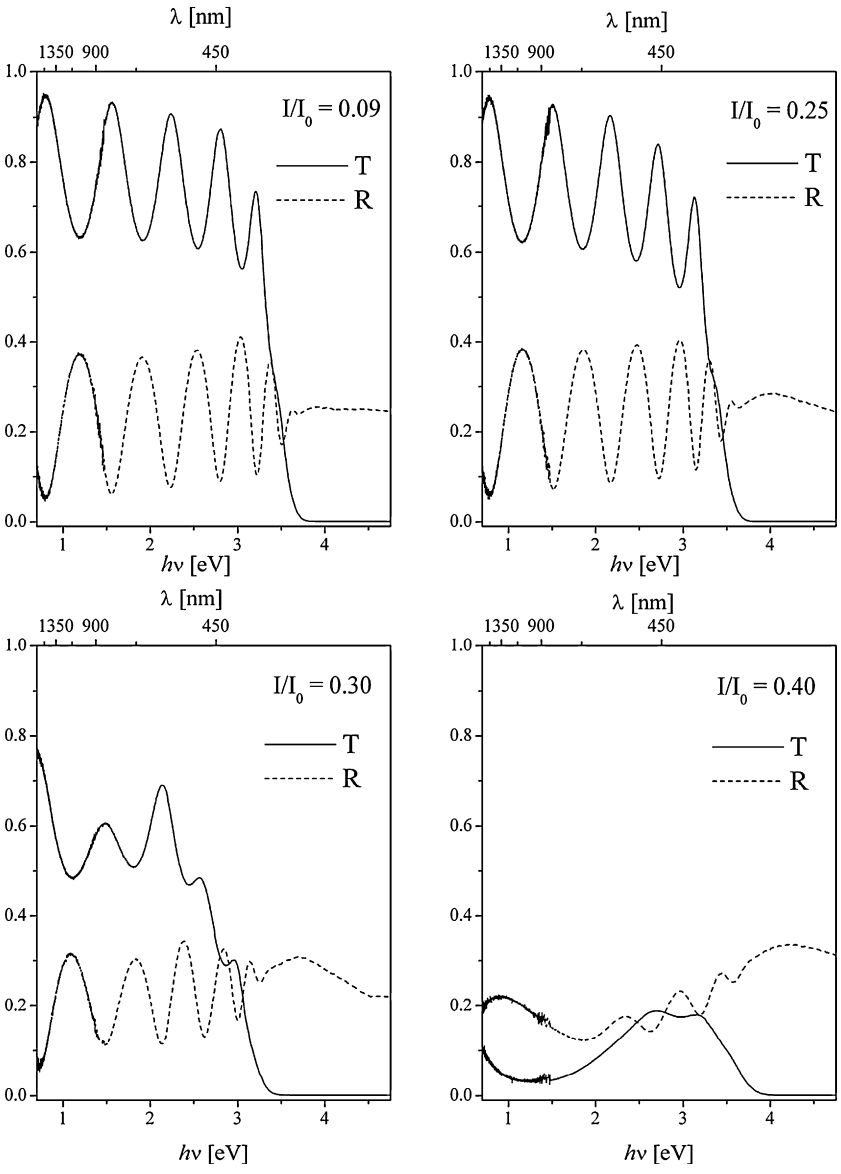


Fig. 4. Spectral dependence of the optical transmittance T and reflectance R for $TiO_2$ thin film photoanodes deposited at transparent substrates at different $I/I_0$.

The photocurrent versus time characteristics for the photoanodes obtained at the highest and the lowest $I/I_0$ are shown in Fig. 5. Immediately after the light is switched on, there is a distinct anodic spike on the $I_{ph}$ versus time curve, caused by additional, photoinduced charge carriers—electrons and holes. At this point, the photocarriers generation rate dominates over the recombination processes within the film. Subsequently, an electric field existing at the photoanode surface region separates efficiently the charge carriers. The holes participate in the oxidation reactions at the film surface (Eq. (2)) and the electrons flow through the external circuit to the cathode, where the reduction reactions take place (Eq. (3)). Then the photocurrent decreases until it reaches a quasi-steady-state, and the photogeneration and recombination rates for the electrode become equal. Switching the light off is followed by a cathodic spike that is assigned to the recombination process involving the electrons from the conduction band and the holes accumulated within the surface region of the semiconducting electrode. One can note that the

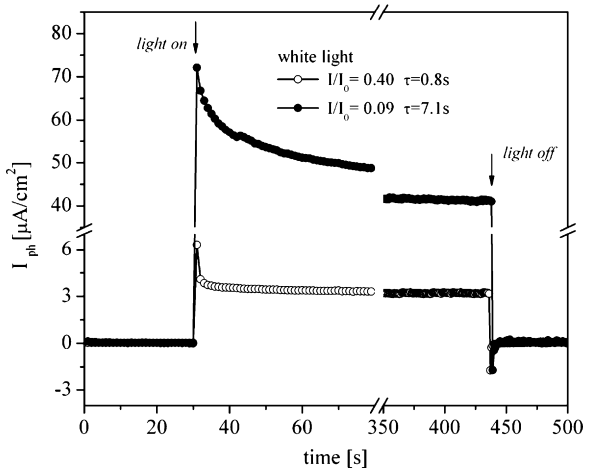


Fig. 5. Transient photocurrent $I_{ph}$ response of $TiO_2$ thin film photoanodes sputtered at $I/I_0 = 0.09$ and 0.40 under white light illumination at 0 V vs. SCE. The arrows indicate when the light was turned on and off.

photocurrent response of the $TiO_2$ photoanode, sputtered from the oxidized target ($I/I_0 = 0.09$), is one order of magnitude higher as compared with that obtained at $I/I_0 = 0.40$. Also, the transient time constant $\tau$, defined in [23], was found to be $0.8 \pm 0.1$ s for the film obtained at $I/I_0 = 0.40$ and $7.1 \pm 0.1$ s for the one sputtered at $I/I_0 = 0.09$. The transient time constant is related to the relaxation time, i.e. the time period needed for the concentration of photocarriers within the film to reach a constant level [23]. Thus, high $I/I_0$ corresponds to a short relaxation time, which is associated probably with a higher number of recombination centres in amorphous films with larger departure from stoichiometry.

Fig. 6 presents the $I_{ph}$–$V$ curves for the $TiO_2$ films deposited at different $I/I_0$. It can be seen that for the films sputtered at $I/I_0 < 0.20$, high anodic photocurrent densities are achieved and the slope of the anodic photocurrent curve for these films is steep, giving evidence for the fast electronic transfer through the photoanode–electrolyte interface. By contrast, the anodic photocurrents recorded for the films sputtered from the less oxidized target ($I/I_0 > 0.25$) are relatively low and do not reach a saturation level.

Another parameter important for the photoanode performance is the flat band potential $V_{fb}$. Generally, the flat band $V_{fb}$ is related to the height of the potential barrier at the photoanode surface region. It should have a highly negative value in order to produce a sufficiently strong electric field, required for the effective separation of the photoinduced electrons and holes. The $V_{fb}$ values found for the films are given in the inset of Fig. 6. A decrease in $I/I_0$ is accompanied by a shift in the $V_{fb}$ towards more negative values.

The IPCE spectral characteristics are shown in Fig. 7. Over the presented spectral range, the photoresponse of the films is determined by the energy band gap of $TiO_2$ and is due to the electron transitions from the valence band to the conduction band. The maximum IPCE values appear at the photon energy $h\nu$ corresponding to the $E_{opt}$ values found from the optical measurements. Similarly to the $I$–$V$ curves, the highest photocurrent, and, as a consequence, the highest IPCE values are obtained for

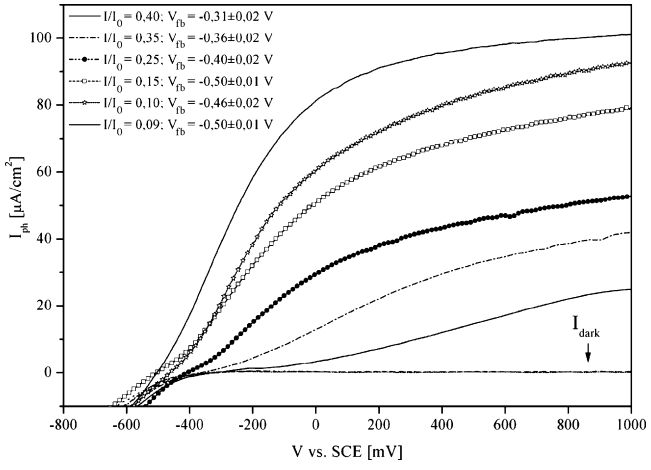


Fig. 6. Photocurrent $I_{ph}$ as a function of a potential $V$ applied to the $TiO_2$ photoanode vs. SCE. The flat band potentials $V_{fb}$ for the photoanodes are listed and the dark currents are also shown.

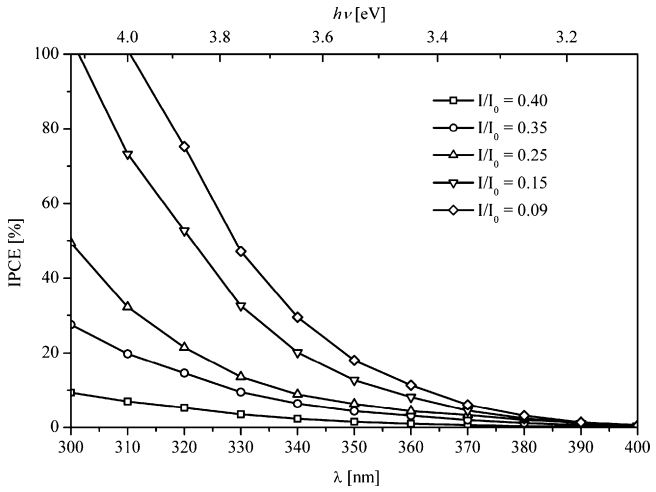


Fig. 7. IPCE vs. wavelength for $TiO_2$ thin film photoanodes sputtered at different $I/I_0$.

the films deposited at $0.09 < I/I_0 < 0.25$. When the target becomes more oxidized, a systematic growth in IPCE is observed.

There are several factors affecting the $TiO_2$ photoresponse, such as the phase composition, crystallization degree and departure from stoichiometry. From the above observations it follows that the best photocurrent dynamic responses are achieved for the titanium dioxide photoanodes deposited from the oxidized target ($I/I_0 = 0.09$), i.e. under the conditions that promote the crystallization with the highest contribution of the anatase. These films are characterized by the highest degree of crystallization. Similar relationship between the microstructure and the photoelectrochemical properties of $TiO_2$ photoanodes was observed for the films deposited at different substrate temperatures $T_s$, where a direct correlation between the $T_s$ and crystallization level existed [24]. Given the fact that the photoelectrochemical properties of $TiO_2$ follow the systematic changes in the oxidation state of the sputtered target surface, reflected by the $I/I_0$ parameter, it can be seen that the microstructure of the photoanode material directly affects the overall PEC performance. It is generally accepted that the $TiO_2$ anatase exhibits higher photocatalytic activity than rutile, therefore an increased contribution of this phase can promote the reactions involved in the photoelectrolysis of water. Moreover, the increase in $I/I_0$ is followed by an increasing departure from stoichiometry and the growing contribution of the amorphous phase. This, in turn, leads to the creation of the additional states within the $TiO_2$ band gap that are responsible for enhanced recombination. As a result, the photocurrent decays quickly and the films obtained at the lowest $I/I_0$ are characterized by extremely low photocurrent densities.

## 4. Conclusions

Systematic study of the $TiO_2$ photoanodes, obtained by means of reactive dc magnetron sputtering within the transition mode was performed. It was found that the microstructure of the films was determined by the sputtering conditions, i.e. the surface state of the target related to the feedback parameter $I/I_0$. The microstructure affected to a large extent the optical and

photoelectrochemical properties of the films. At $I/I_0 < 0.25$, when the target was oxidized, the sputtering process yielded well-crystallized, anatase-rich $TiO_2$ films, characterized by a high efficiency of water photolysis. An increase in $I/I_0$ yields amorphous films with finely dispersed rutile grains. An additional absorption band for the films deposited at $I/I_0 > 0.25$ was formed at about 1–2 eV. Simultaneously, the photocurrent density was lowered and the efficiency of photolysis process decreased. We believe that degradation of the photoanodic properties of the films with the increasing $I/I_0$ is caused by the departure from stoichiometry and a growing contribution of the amorphous phase. As a result, the additional states within the $TiO_2$ forbidden energy gap occur. In our opinion these additional states are responsible for the recombination processes and, consequently, fast photocurrent decay.

## Acknowledgement

This work was supported by Polish Ministry of Education and Science grant no. 3T08D 054 30.

## References

[1] M. Momirlan, T.N. Veziroglu, Renew. Sust. Energy Rev. 6 (2002) 141–179.
[2] J.R. Bolton, Sol. Energy 57 (1996) 37–50.
[3] S. Chandra, R.K. Pandey, Phys. Stat. Sol. A 72 (1982) 415–454.
[4] O. Carp, C.L. Huisman, A. Reller, Prog. Solid State Chem. 32 (2004) 33–177.
[5] A. Fujishima, K. Honda, Nature 238 (1972) 37–38.
[6] M. Radecka, Thin Solid Films 451–452 (2004) 98–104.
[7] Ch.J. Barbe, F. Arendse, P. Comte, M. Jirousek, F. Lenzmann, V. Shklover, M. Gratzel, J. Am. Ceram. Soc. 80 (1997) 3157–3171.
[8] T. Yoko, L. Hu, H. Kozuka, S. Sakka, Thin Solid Films 283 (1996) 188–195.
[9] Y. Li, J. Hagen, W. Schaffrath, P. Otschik, D. Haarer, Sol. Energy Mater. Sol. Cells 56 (1999) 167–174.
[10] G. Balasubramanian, D.D. Dionysiou, M.T. Suidan, V. Subramanian, I. Baudin, J.M. Laine, J. Mater. Sci. 38 (2003) 823–831.
[11] M. Yamagishi, S. Kuriki, P.K. Song, Y. Shigesato, Thin Solid Films 442 (2003) 227–231.
[12] Y.-L. Choi, S.-H. Kim, Y.-S. Song, D.Y. Lee, J. Mater. Sci. 39 (2004) 5695–5699.
[13] J. Ebisawa, E. Ando, Curr. Opin. Solid State Mater. Sci. 3 (1998) 386–389.
[14] P. Baroch, J. Musil, J. Vlcek, K.H. Nam, J.G. Han, Surf. Coat. Technol. 193 (2005) 107–111.
[15] D. Carter, W.D. Sproul, D. Christie, Proceedings of the Society of Vacuum Coaters 46th Annual Technical Conference, Soc. Vacuum Coaters, Albuquerque, 2003, pp. 23–28.
[16] A. Brudnik, H. Czternastek, K. Zakrzewska, M. Jachimowski, Thin Solid Films 199 (1991) 45–48.
[17] R. Dannenberg, P. Greene, Thin Solid Films 360 (2000) 122–127.
[18] M. Radecka, K. Zakrzewska, H. Czternastek, T. Stapiński, Appl. Surf. Sci. 65–66 (1993) 227–234.
[19] K. Zakrzewska, Titanium Dioxide Thin Films for Gas Sensors and Photonic Applications, AGH Univ. Sci. Technol., Krakow, 2003, pp. 68–75.
[20] J. Tauc, Mater. Res. Bull. 5 (1970) 721–726.
[21] W.P. Gomes, in: H.S. Nalva (Ed.), Handbook of Advanced Electronic and Photonic Materials and Devices, vol. 1: Semiconductors, Academic Press, San Diego CA, 2000, pp. 147–249.
[22] H. Gerischer, in: F. Cardona, W.P. Gomes, W. Dekeyser (Eds.), Photovoltaic and Photoelectrochemical Solar Energy Conversion, Plenum Press, New York, 1981, pp. 199–245.
[23] D. Tafalla, P. Salvador, R.M. Benito, J. Electrochem. Soc. 137 (1990) 1810–1815.
[24] M. Radecka, K. Zakrzewska, A. Gorzkowska-Sobas, E. Kusior, Surf. Sci. 600 (2006) 3964–3970.